RESEARCH ARTICLE
doi: 10.2306/scienceasia1513-1874.2026.063

ScienceAsia 52 (4): 2026: ID 2026063: **1–10**

Unveiling the size effect of boron nitride nanosheets in electrospun PVA composites: towards superior in-plane thermal conductivity

Shanshan Chao[a], **Zihan Teng**[a], **Liangjun Shen**[b], **Lejia Wang**[b,*], **Xing Li**[a,*]

[a] School of Materials Science and Chemical Engineering, Ningbo University, Ningbo, Zhejiang 315211 China
[b] School of Material and Chemical Engineering, Ningbo University of Technology, Ningbo, Zhejiang 315211 China

*Corresponding authors, e-mail: wanglejia@nbut.edu.cn, lixing@nbu.edu.cn

Received 12 Feb 2026, Accepted 2 Jun 2026
Available online 19 Jul 2026

ABSTRACT: Developing advanced heat spreaders with high in-plane thermal conductivity is critical for modern electronics. Herein, we report a hierarchical alignment strategy to fabricate polyvinyl alcohol (PVA)/boron nitride nanosheet (BNNS) composite films via electrospinning and subsequent hot-pressing. By systematically regulating the lateral size of BNNSs, we unveil a decisive size effect on phonon transport within the confinement of nanofibers. Our findings demonstrate that an optimal filler size of 4 µm strikes a critical balance between minimizing interfacial phonon scattering and maintaining structural integrity. The synergistic effect of shear-induced alignment and densification constructs highly ordered phonon highways, enabling the composite with 70 wt% loading to achieve an exceptional in-plane thermal conductivity of 25.58 $W\,m^{-1}\,K^{-1}$. Furthermore, the films exhibit excellent mechanical flexibility and rapid heat dissipation capability, as confirmed by infrared thermal imaging. This work provides fundamental insights into the interplay between filler dimensions and confinement effects, offering a scalable route for high-performance thermal management materials.

KEYWORDS: boron nitride nanosheets, electrospinning, polyvinyl alcohol, in-plane thermal conductivity, composite material

INTRODUCTION

Efficiently dissipating concentrated waste heat has become a critical thermal management challenge due to the rapid miniaturization, integration, and flexibility of modern electronics, such as wearables and foldable screens [1–3]. Unlike traditional rigid electronics, these next-generation devices require heat spreaders that not only possess exceptional in-plane thermal conductivity to rapidly diffuse local hot spots but also exhibit lightweight, electrical insulation, and mechanical flexibility to accommodate complex deformation [4]. While metals like copper and aluminum are excellent heat conductors, their high density, lack of flexibility, and electrical conductivity severely restrict their application in lightweight and compact electronic packages where electrical short-circuiting is a major concern [5]. Consequently, polymer-based composites have emerged as promising alternatives. However, the inherently low thermal conductivity of most polymers remains a fundamental bottleneck, necessitating the incorporation of thermally conductive fillers to construct efficient heat dissipation networks [6–8].

To address this limitation, various inorganic fillers such as alumina (Al_2O_3), aluminum nitride (AlN), and graphene have been extensively explored [9, 10]. Among these, hexagonal boron nitride nanosheets (BNNSs) stand out as the ideal candidate for advanced insulating heat spreaders [11]. Compared to traditional ceramic fillers such as Al_2O_3 and AlN, BNNSs offer a unique combination of properties. They possess a graphite-like layered structure that imparts ultrahigh intrinsic in-plane thermal conductivity and a low dielectric constant, yet they are significantly lighter, enabling the fabrication of lightweight thermal management components [12–14]. Nevertheless, the full potential of BNNSs is rarely realized in conventional blending processes, where random filler orientation leads to discontinuous phonon transport pathways and excessive interfacial scattering [15, 16]. To maximize the in-plane thermal conductivity required for heat spreaders, it is imperative to align the 2D BNNSs along the planar direction, thereby constructing continuous "phonon highways" that facilitate rapid lateral heat diffusion [17, 18].

In the pursuit of such highly oriented and flexible structures, electrospinning has garnered significant attention as a powerful structural regulation technique [19]. Unlike casting or filtration methods, electrospinning generates continuous nanofibers through a strong electric field, which not only induces the directional alignment of fillers along the fiber axis via shear and confinement effects but also creates a naturally flexible non-woven network [20, 21]. This unique feature makes electrospun composites particularly suitable for flexible electronics, where the material must withstand bending and folding without structural failure [22]. While the alignment capability of electrospinning is well recognized, a critical scientific gap remains in optimizing the dimensional matching between the 2D BNNS fillers and the 1D host nanofibers. The lateral size of the filler is a decisive factor in phonon transport;

however, how the filler size influences the alignment degree, encapsulation efficiency, and ultimate thermal performance within the confined space of electrospun fibers has not been systematically elucidated [23].

Motivated by these considerations, this study presents a robust strategy to fabricate lightweight, flexible, and highly thermally conductive PVA/BNNS composite films designed specifically for lateral heat dissipation. We employ a hierarchical alignment approach combining co-electrospinning with a subsequent hot-pressing densification process. The electrospinning stage achieves an axial pre-alignment of BNNSs within the nanofibers, while hot-pressing transforms the porous fiber mat into a dense, nacre-like layered structure, further promoting planar stacking and interconnection. Distinct from previous works, we rigorously investigate the size effect of BNNSs (ranging from 0.5 to 8 μm) on the microstructural evolution and thermal properties of the composites. We demonstrate that optimizing the filler dimension is crucial for minimizing interfacial thermal resistance while maintaining structural integrity. The resulting composite film, with an optimized BNNS size of 4 μm and a high loading of 70 wt%, exhibits superior in-plane thermal conductivity and excellent mechanical flexibility, offering a promising solution for thermal management in high-power density and flexible electronic devices.

MATERIALS AND METHODS

Materials

Polyvinyl alcohol (PVA, MW = 205000) was purchased from Aladdin Biochemical Technology Co., Ltd. (Shanghai, China). Hexagonal boron nitride (h-BN) powders with an average particle size of 30 μm were procured from Dandong Chemical Industry Research Institute (Liaoning, China). Isopropyl alcohol (IPA) was obtained from Sinopharm Chemical Reagent Co., Ltd. (Shanghai, China). Deionized (DI) water was generated using a laboratory water purification system and used throughout the experiments. All chemicals were used as received without further purification.

Preparation of size-controlled BNNSs

Boron nitride nanosheets (BNNSs) with tunable lateral dimensions were prepared via a liquid-phase exfoliation method assisted by high-pressure homogenization [24]. In a typical procedure, pristine h-BN powders were dispersed in a binary solvent mixture of IPA and DI water (4:6 v/v) to achieve an initial concentration of 10 mg/ml. The suspension was pre-mixed and then subjected to shear exfoliation using a high-pressure homogenizer (AH-100D, ATS Engineering Inc., Shanghai, China).

To systematically regulate the lateral size of the BNNSs, the homogenization pressure and the number of circulation cycles were precisely controlled. Specifically, BNNS-8 μm was processed at 50 MPa for 20 cycles; BNNS-4 μm was processed at 75 MPa for 20 cycles; BNNS-2 μm was processed at 100 MPa for 40 cycles; and BNNS-0.5 μm was processed at 180 MPa for 40 cycles. The resulting dispersions were vacuum filtered through a polytetrafluoroethylene (PTFE) membrane (pore size: 0.22 μm) and washed extensively with DI water to remove residual solvents. Finally, the collected filter cakes were freeze-dried for 48 h to obtain dry BNNS powders.

Fabrication of PVA/BNNS composite films

The highly oriented PVA/BNNS composite films were fabricated using a combination strategy of co-electrospinning and hot-pressing.

Spinning solution preparation: First, a 20 wt% PVA aqueous solution was prepared by dissolving PVA granules in DI water at 80 °C for 30 min under continuous stirring. Separately, a calculated amount of BNNS powder was dispersed in DI water and magnetically stirred for 6 h at room temperature to ensure initial dispersion. The PVA stock solution was then slowly added to the BNNS suspension. The mixture was vigorously stirred for 12 h and subsequently ultrasonicated for 20 min (400 W, ice bath) to yield a homogeneous, bubble-free spinning dope with a final PVA concentration of 7 wt%. The mass ratio of BNNS to PVA was adjusted to achieve varying filler loadings (30, 40, 50, 60, and 70 wt% relative to the total solid content).

Electrospinning process: The precursor solution was loaded into four 5 ml syringes equipped with 21G stainless steel needles. The syringes were mounted on a syringe pump and arranged in an opposing configuration to ensure uniform fiber deposition. Electrospinning was performed under the following optimized conditions: applied voltage of 22 kV, tip-to-collector distance of 20 cm, and a solution feed rate of 0.5 ml/h. The nanofibers were collected onto a high-speed rotating drum collector (2500 rpm) to induce axial alignment. The environmental temperature and relative humidity were strictly controlled at 25 ± 2 °C and 50–55%, respectively.

Hot-pressing densification: After 4 h of collection, the as-spun nanofiber mats were peeled off and cut into 4×4 cm^2. To construct a dense film with sufficient thickness, eight layers of these mats were stacked in a cross-ply configuration to ensure uniform in-plane thermal conductivity. The assembly was then hot-pressed at 100 °C under a pressure of 30 MPa for 10 min. This process eliminated inter-fiber voids and fused the PVA matrix, resulting in a compact composite film with a thickness of approximately 30 μm.

Characterization

Morphology and structure: The microscopic morphologies of the exfoliated BNNSs and the cryo-fractured surfaces of the composite films were characterized by

field-emission scanning electron microscopy (FESEM; SU8100, Hitachi, Tokyo, Japan) at an accelerating voltage of 10 kV. The lateral size distribution of BNNSs was statistically analyzed by measuring over 100 individual sheets using Nano Measurer 1.2 software. Crystal structures were analyzed by X-ray diffraction (XRD; D8 Advance, Bruker, Germany). Chemical structures were verified using Fourier-transform infrared spectroscopy (FT-IR; Vertex 70, Bruker) via the KBr pellet method over a wavenumber range of 4000–500 cm^{-1}.

Thermal properties: The thermal stability of the composites was evaluated using thermogravimetric analysis (TGA; TGA/DSC, Mettler Toledo, Zurich, Switzerland) from 25 to 800 °C at a heating rate of 20 °C/min under an oxygen atmosphere. The in-plane thermal conductivity was measured at room temperature using a Hot Disk Thermal Constants Analyzer (TPS 3500, Hot Disk AB, Gothenburg, Sweden) equipped with an anisotropic module, based on the transient plane source method. During the measurement, the Hot Disk sensor probe, consisting of a thin electrically insulating film-encapsulated metal spiral that acts as both the heat source and temperature sensor, was sandwiched between two identical sample pieces to minimize contact resistance.

Infrared thermography: To visualize the heat-spreading performance, the surface temperature evolution of the films was monitored using an infrared thermal imager (FLIR A655sc). Samples were placed on a constant heat source (or heated at one end), and thermal images were captured in real time to record the temperature distribution profiles.

RESULTS AND DISCUSSION

Design strategy and microstructural evolution mechanism

The fabrication strategy and structural design of the PVA/BNNS composite films are schematically illustrated in Fig. 1. This work aims to address the trade-off between filler network connectivity and processability by establishing a hierarchical alignment structure. The process comprises two critical stages: the controlled preparation of BNNS building blocks (Fig. 1a) and the assembly of ordered thermal conductive networks (Fig. 1b).

Controlled exfoliation of BNNSs (Fig. 1a): The first stage focuses on the precise dimensional regulation of the fillers. As depicted in Fig. 1a, we employed a high-pressure homogenization technique to exfoliate bulk h-BN into nanosheets. The core hypothesis here is that the lateral size of the BNNSs is a determinant factor in phonon transport. By manipulating the shear intensity (pressure) and duration (cycles), we aimed to obtain BNNSs with distinct lateral dimensions ranging from sub-micron to several microns. This size controllability is essential to systematically investigate the size effect, specifically how the aspect ratio of the filler influences the balance between interfacial thermal resistance and network percolation within the confined polymer matrix [25].

Hierarchical alignment via electrospinning and hot-pressing (Fig. 1b): To maximize the in-plane thermal conductivity, we proposed a two-step "shear-induced alignment" and densification strategy (Fig. 1b). During the co-electrospinning process, the electrostatic stretching force and rapid solvent evaporation impose a strong hydrodynamic shear field on the spinning jet. We anticipated that this shear field will exert a torque on the 2D BNNS platelets, compelling them to align their basal planes parallel to the axis of the 1D PVA nanofibers. This confinement effect is designed to pre-order the fillers, overcoming the random orientation typical of solution casting.

Subsequently, the hot-pressing treatment serves to eliminate the insulating air voids inherent in the non-woven mats and apply vertical compression. This step was expected to further reorient the BNNS-encapsulated nanofibers into the horizontal plane, transforming the fibrous network into a dense, nacre-like layered structure.

Proposed mechanism of size-dependent thermal conduction: The schematic diagrams at the bottom of Fig. 1b illustrate our theoretical model regarding the impact of BNNS size on thermal transport efficiency: Small-sized BNNSs: We hypothesized that while small sheets could be easily aligned, their discrete distribution would create a high density of filler-polymer interfaces. Phonons must frequently cross these scattering boundaries, leading to high total interfacial thermal resistance and limited thermal conductivity. Medium-sized BNNSs: As the size increases to an optimal range, the BNNSs were expected to act as effective thermal bridges. The increased aspect ratio should facilitate the formation of sheet-to-sheet overlaps, creating continuous phonon highways that allow heat to bypass the insulating matrix. Large-sized BNNSs: However, excessively large fillers may encounter confinement mismatch issues. We postulated that if the BNNS size exceeded the nanofiber diameter, it might disrupt the spinning process or lead to poor encapsulation, resulting in structural defects that hinder effective network formation.

Therefore, identifying the optimal BNNS size that balances interfacial resistance with structural integrity is the central goal of this study. To validate this design strategy and the proposed mechanism, we first characterized the morphology and size distribution of the prepared BNNSs.

Morphological characterization and size distribution of BNNSs

To validate the efficacy of the high-pressure homogenization technique in regulating filler dimensions, the morphology and size distribution of the exfoliated BNNSs were systematically characterized. As shown

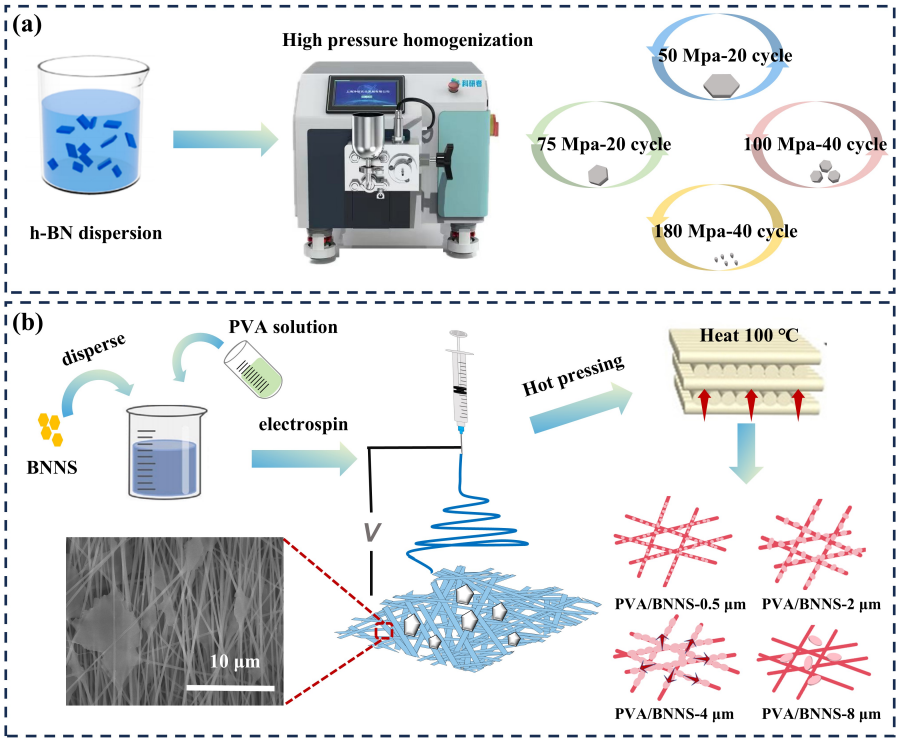

Fig. 1 Schematic diagram of the preparation of PVA/BNNS composite films with interconnected and oriented BNNSs.

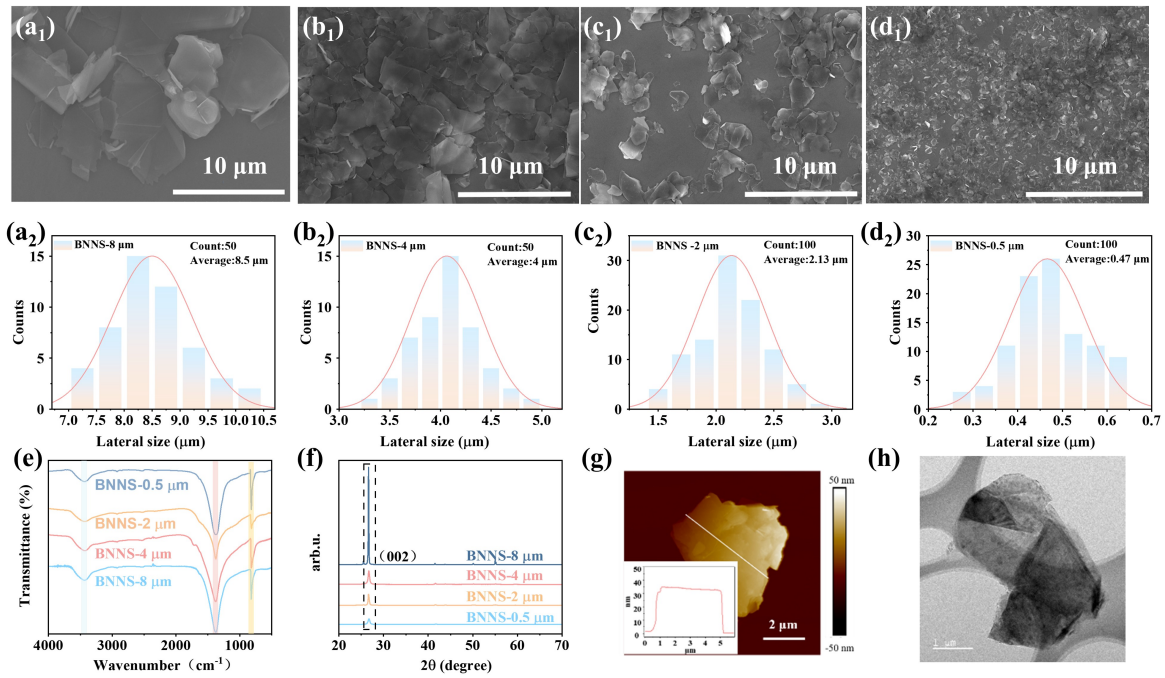

Fig. 2 Morphology, microstructure, and size distribution of BNNSs. (a1–d2) SEM images and corresponding lateral size distribution histograms of BNNSs prepared under different homogenization conditions: (a1–a2) BNNS-8 μm, (b1–b2) BNNS-4 μm, (c1–c2) BNNS-2 μm, and (d1–d2) BNNS-0.5 μm. (e) FTIR spectra of the exfoliated BNNSs, confirming the preservation of chemical structure. (f) XRD patterns showing the characteristic diffraction peaks of h-BN; the intensity of the (002) peak decreases with reducing lateral size. (g) AFM image and the inset showing the thickness distribution of the BNNS-4 μm. (h) The TEM image of BNNS-4 μm.

in the FESEM images (Fig. 2a_1–d_1), the bulk h-BN precursors were successfully exfoliated into ultrathin nanosheets with smooth surfaces and sharp edges. Crucially, by modulating the homogenization intensity, four distinct size populations were obtained. The corresponding statistical analyses (Fig. 2a_2–d_2) reveal that the average lateral sizes of the BNNSs were controlled at approximately 8.5, 4.0, 2.13, and 0.47 µm, respectively. This precise size tunability provides a reliable platform for the subsequent investigation of size-dependent phonon transport.

The structural integrity of the BNNSs following the intense physical exfoliation was further verified. The FTIR spectra (Fig. 2e) for all samples display identical characteristic absorption peaks at ∼1370 cm^{-1} and ∼810 cm^{-1}, corresponding to the in-plane B—N stretching and out-of-plane B—N—B bending vibrations, respectively [26]. This indicates that the chemical bonding of the h-BN lattice remained intact. Consistent with this, the XRD patterns (Fig. 2f) exhibit the typical diffraction peaks of hexagonal boron nitride. Notably, a gradual attenuation in the intensity of the (002) diffraction peak was observed as the lateral size decreased [27]. This phenomenon is attributed to the reduction in the number of stacking layers along the c-axis and a partial loss of long-range order due to the shear forces, while the unchanged peak positions suggest that the in-plane crystallinity—critical for thermal conduction—was well-preserved. Additionally, AFM characterization of the representative BNNS-4 µm sample (Fig. 2g) confirmed a flat nanosheet morphology with a thin thickness, indicating a high aspect ratio favorable for constructing thermal networks. The TEM image clearly reveals the typical two-dimensional (2D) nanosheet morphology of boron nitride (BN) (Fig. 2h). The nanosheets exhibit distinct edges and a semi-transparent appearance, indicating that the bulk h-BN has been successfully exfoliated into thin nanosheets with a lateral size of approximately 4 µm via high-pressure homogenization.

Structural characterization of electrospun PVA/BNNS composite film

Having established the quality of the fillers, we examined the microstructural evolution of the as-spun PVA/BNNS composite films (before hot-pressing) to elucidate the interaction between filler size and fiber confinement. Fig. 3a shows that pure PVA forms a smooth, uniform, and randomly oriented non-woven nanofiber network. Upon incorporating 70 wt% BNNSs, the fiber morphology exhibits a distinct size-dependent evolution. For composites containing small BNNSs (0.5 and 2 µm, Fig. 3b,c), the nanofibers remain relatively smooth with the fillers fully encapsulated within the polymer matrix. The confinement effect of electrospinning is evident, as the nanosheets are constrained to align along the fiber axis; however, their small dimensions result in a discrete distribution with limited interconnectivity.

As the filler size increases to 4 µm (Fig. 3d), a transition to a bamboo-like morphology occurs, characterized by periodic nodes where the larger BNNSs are embedded. Despite the increased size, these fillers remain predominantly oriented along the fiber direction, suggesting that the hydrodynamic shear forces in the spinning jet are sufficient to align them. However, when the size is further increased to 8 µm (Fig. 3e), the structural integrity of the fibers begins to deteriorate. The lateral size of these fillers approaches or exceeds the diameter of the nanofibers, leading to significant protrusions and defects where BNNSs are only partially encapsulated. This dimensional mismatch disrupts the continuity of the fiber network and creates interfacial voids.

The impact of these microstructural differences on phonon transport is quantified in Fig. 3f. Pure PVA exhibits a low in-plane thermal conductivity (TC) of 4.43 $W\,m^{-1}\,K^{-1}$. The addition of 70 wt% BNNSs significantly enhances the TC, but a non-monotonic trend is observed with respect to filler size. The TC increases from 14.03 $W\,m^{-1}\,K^{-1}$ for the 0.5 µm sample to a peak of 25.58 $W\,m^{-1}\,K^{-1}$ for the 4 µm sample. This enhancement is attributed to the increased aspect ratio, which reduces the density of filler-matrix interfaces and facilitates the formation of longer continuous thermal pathways. Conversely, the TC drops to 24.3 $W\,m^{-1}\,K^{-1}$ for the 8 µm sample. This decline correlates with the structural defects observed in SEM, where poor encapsulation and interfacial voids act as phonon scattering centers, counteracting the benefits of the larger filler size. Consequently, the 4 µm BNNSs demonstrate the optimal balance between aspect ratio and processability, achieving the highest thermal conductivity among the as-spun samples. With the optimal filler size identified, the subsequent section will focus on optimizing the BNNS loading content to further maximize the thermal performance.

Influence of BNNS loading content on morphology and thermal properties

Building upon the optimization of filler size in the previous section, where 4 µm BNNSs were identified as the ideal building blocks, we proceeded to investigate the impact of filler loading content (ranging from 30 to 70 wt%) on the microstructural evolution and thermal performance of the composites. The SEM images of the as-spun nanofiber mats (Fig. 4a–c) demonstrate the robustness of the electrospinning process even at high solid loadings. Remarkably, the "bamboo-like" fiber morphology is well-preserved across all concentrations, without any signs of jet instability or structural collapse. The 4 µm BNNSs are effectively encapsulated within the PVA matrix and aligned along the fiber axis, confirming that the optimized aspect ratio of the filler is compatible with the electrospinning of high-concentration dopes.

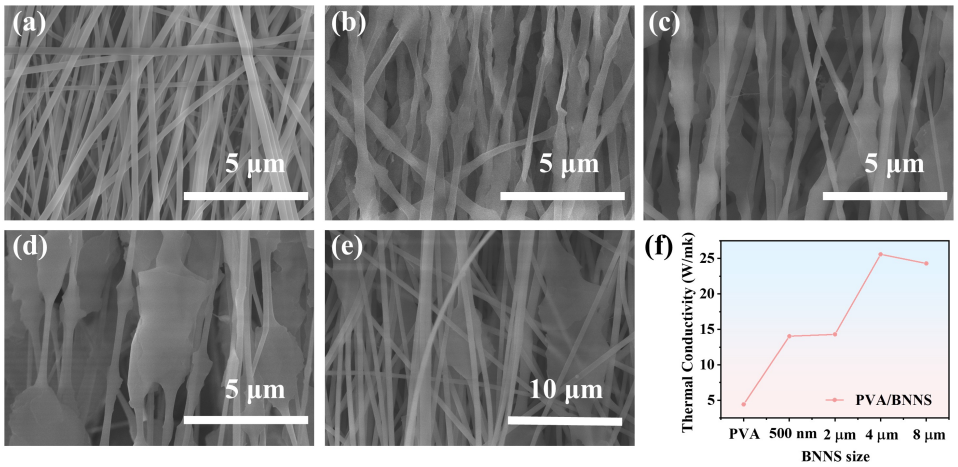

Fig. 3 Structure and morphology of as-spun PVA/BNNS composite films before hot-pressing. (a) SEM image of pure PVA nanofiber film. (b–e) SEM images of PVA/BNNS composite films with a fixed BNNS loading of 70 wt% but varying filler sizes: (b) 0.5 µm, (c) 2 µm, (d) 4 µm, and (e) 8 µm. (f) In-plane thermal conductivity (TC) of pure PVA and PVA/BNNS composite films as a function of BNNS lateral size.

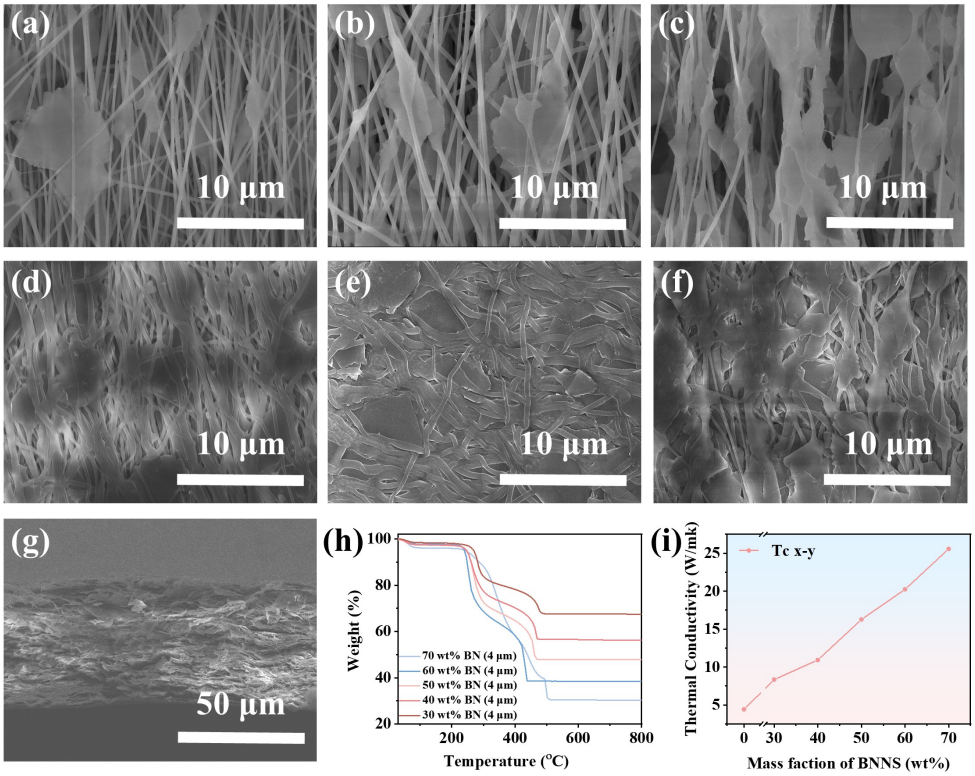

Fig. 4 Structure, thermal stability, and thermal conductivity of PVA/BNNS composite films with varying BNNS-4 µm loadings. (a–c) SEM images of as-spun nanofiber mats with BNNS-4 µm loadings of 30 wt%, 40 wt%, and 70 wt%, respectively, showing well-preserved fiber morphology. (d–f) Surface SEM images of the corresponding composite films after hot-pressing at 100 °C and 30 MPa, revealing a dense and uniform texture. (g) Cross-sectional SEM image of the 70 wt% composite film, displaying a highly oriented, nacre-like layered architecture. (h) TGA curves of PVA/BNNS composites with different filler loadings, indicating enhanced thermal stability. (i) In-plane thermal conductivity (TC) as a function of BNNS-4 µm mass fraction, demonstrating a non-linear increase due to the formation of a percolated network.

Following the hot-pressing treatment at 100 °C and 30 MPa, the porous nanofiber networks were transformed into dense, solid films, as evidenced by the surface morphologies in Fig. 4d–f. The application of heat and pressure facilitated the fusion of the PVA matrix, eliminating the interstitial voids between fibers while retaining the horizontal alignment of the BNNSs. As the filler content increases from 30 wt% to 70 wt%, the surface reveals a progressively denser packing of nanosheets. Despite the high loading, the films remain smooth and uniform, indicating excellent interfacial compatibility between the hydroxyl-rich PVA and the BNNSs. The internal structural ordering is further elucidated by the cross-sectional SEM image of the 70 wt% composite film (Fig. 4g). A highly anisotropic, nacre-like layered structure is clearly visible, where the BNNSs are stacked parallel to the film plane and separated by ultrathin layers of PVA. This architecture is thermodynamically favorable for phonon transport, as it maximizes the in-plane contact area between adjacent nanosheets while minimizing the vertical thermal resistance, effectively creating phonon highways along the planar direction [25, 28].

The incorporation of BNNSs also significantly enhances the thermal stability of the composites, a critical factor for their application in high-temperature environments. The TGA curves (Fig. 4h) show that pure PVA undergoes rapid degradation starting around 250 °C, attributed to the elimination of side hydroxyl groups and subsequent main-chain scission. In contrast, the decomposition temperatures of the composites shift systematically to higher values with increasing BNNS loading. The residual weight at 600 °C is directly proportional to the filler content, corroborating the nominal loading values. This improvement is ascribed to the barrier effect of the high-aspect-ratio BNNSs, which create a tortuous path that retards the diffusion of volatile decomposition products and effectively shields the underlying polymer matrix from thermal flux.

The culmination of these structural optimizations is reflected in the thermal conductivity performance. Fig. 4i summarizes the in-plane thermal conductivity (TC) of the composite films as a function of BNNS-4 loading. The TC exhibits a distinct non-linear, exponential growth pattern consistent with percolation theory. At lower loadings (< 40 wt%), the increase in TC is moderate, as the BNNSs are relatively isolated by the polymer matrix, preventing the formation of continuous conductive pathways. However, as the loading approaches and exceeds 50 wt%, the TC surges, reaching a remarkable value of 25.58 $W\,m^{-1}\,K^{-1}$ at 70 wt%. This dramatic enhancement signifies the transition from a matrix-dominated regime to a filler-dominated percolation regime. At this high concentration, the average inter-particle distance is minimized, and the probability of sheet-to-sheet overlap is maximized. The highly aligned and densely packed 4 μm BNNSs form an extensive, interconnected thermal network that effectively bridges the insulating PVA matrix, facilitating rapid and efficient phonon transport across the macroscopic dimensions of the film [29].

Mechanical flexibility and thermal conduction mechanism

For practical applications in next-generation flexible electronics, thermal interface materials must possess a dichotomous combination of properties: ultrahigh thermal conductivity typically associated with rigid ceramics and exceptional mechanical compliance characteristic of polymers [30]. Generally, incorporating high loadings of inorganic fillers (exceeding 50 wt%) into a polymer matrix inevitably leads to severe embrittlement and a catastrophic loss of processability. However, the PVA/BNNS composite films fabricated in this study defy this trade-off. As demonstrated in Fig. 5a,b, at a 70 wt% loading of 4 μm BNNSs, the as-spun PVA/BNNS electrospun membrane exhibits a tensile strain of 150% and a tensile stress of 10.5 MPa. The robust mechanical performance of the electrospun fibers is primarily attributed to the relatively uniform dispersion of BNNS fillers within the PVA matrix. Specifically, the PVA matrix enhances interfacial adhesion, enabling the BNNS fillers to effectively transfer stress and inhibit crack propagation, thereby improving the tensile strength. However, following the stacking and hot-pressing process, the tensile strain and stress of the PVA/BNNSs composite film decrease to 80% and 7.5 MPa, respectively. This degradation is ascribed to the tendency of BNNS fillers to aggregate after hot-pressing, which creates excessive stress concentration sites and leads to a decline in mechanical strength. And even at a substantial filler loading of 70 wt%, the composite film exhibits remarkable flexibility and macroscopic integrity. It can be effortlessly bent, twisted, and folded without fracturing or delaminating. This mechanical robustness is quantitatively supported by the tensile test results in Fig. 5b, which show that the film retains a respectable tensile strength and elongation at break despite the dominance of the inorganic phase. This unusual flexibility is attributed to the unique brick-and-mortar nacre-like architecture constructed via the hierarchical alignment strategy. The highly aligned BNNSs (bricks) act as rigid stress-bearing units, while the thin layers of PVA (mortar) provide energy dissipation through chain slippage. Furthermore, the abundant hydroxyl groups on the PVA chains form extensive hydrogen bonding networks with the functionalized surfaces of the BNNSs, ensuring strong interfacial adhesion and effective stress transfer during deformation.

However, a noticeable decline in the mechanical flexibility of composite films was observed after hot-pressing. The underlying mechanisms are summarized as follows: First, densification and porosity reduction: the as-spun nanofibers initially form a loose, non-

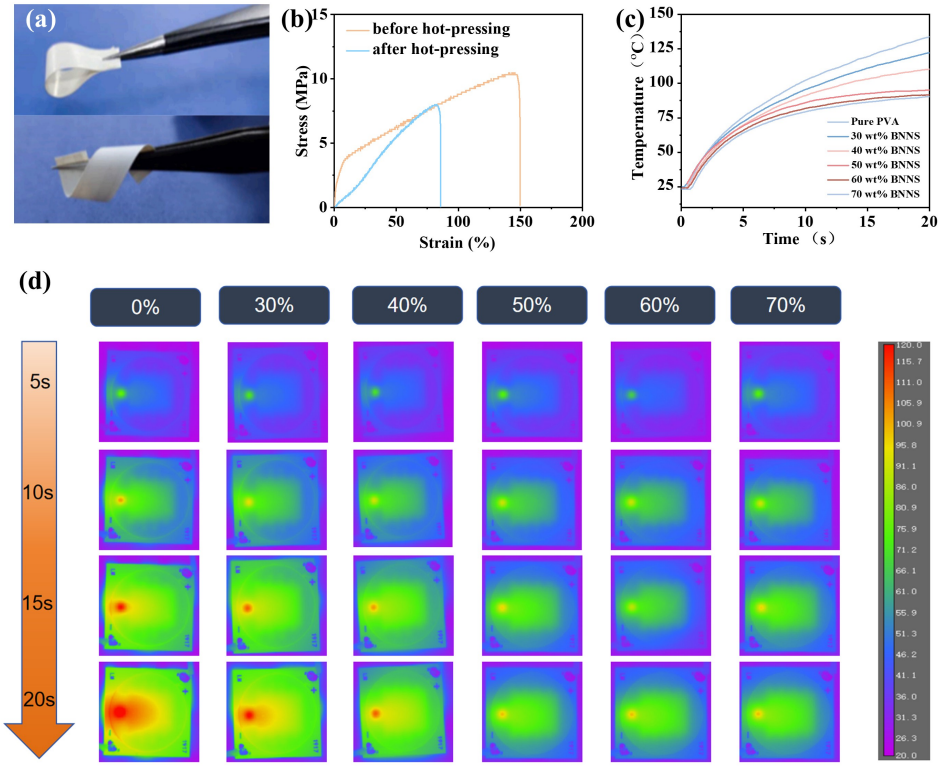

Fig. 5 Mechanical flexibility and thermal management performance of PVA/BNNS-4 µm composite films. (a) Digital photographs demonstrating the excellent flexibility of the composite film with 70 wt% BNNS loading, which can withstand bending and folding without fracture. (b) Tensile stress-strain curves of the 70 wt% composite film, highlighting its mechanical robustness. (c) Infrared thermal images of pure PVA and composite films with varying BNNS loadings recorded at different time intervals during heating, visualizing the lateral heat spreading capability. (d) Time-dependent surface temperature profiles extracted from the IR images, confirming the superior thermal response and heat dissipation efficiency of the 70 wt% composite film.

woven porous structure with significant free volume, which facilitates easy fiber sliding and bending. Hot-pressing collapses these pores, creating a highly dense film where the physical entanglement of fibers is replaced by a fused, continuous matrix, inherently increasing stiffness and reducing macroscopic flexibility. Second, increased filler-matrix interfacial constraint: upon densification, the BNNSs are forced into closer contact with the PVA chains. The high-aspect-ratio BNNSs act as rigid reinforcing walls that significantly restrict the mobility of polymer chains, leading to a transition from a flexible textile-like behavior to a more rigid film-like behavior. Third, crystallinity changes: the simultaneous application of heat and pressure during hot-pressing promotes the re-crystallization of PVA chains. Increased crystallinity, while beneficial for thermal transport, typically results in a more brittle mechanical response [31].

To validate the efficacy of these composites as high-performance heat spreaders in real-world scenarios, their thermal management capability was visualized using infrared (IR) thermography. PVA/BNNS composite films and pure PVA films of identical dimensions and thickness were placed on a constant-temperature heating plate at 130 °C, and their surface temperature variations were monitored via infrared (IR) thermography (Fig. 5c). Within 20 s, the surface temperature of the pure PVA film surged from 25 °C to 130 °C, whereas the 70 wt% PVA/BNNS composite film only reached 90 °C over the same duration. This significantly lower steady-state temperature demonstrates that the PVA/BNNS composite films possess superior in-plane thermal diffusion capabilities. As demonstrated in Fig. 5d, the pure PVA membrane exhibits a pronounced hot spot phenomenon, where heat accumulates locally due to its poor thermal conductivity, resulting in a steep temperature gradient and a high peak temperature. In sharp contrast, the composite films, particularly the ones with 70 wt% BNNS-4 µm, display a rapid and uniform temperature distribution across the entire surface. The heat generated at the source is efficiently spread laterally to the cooler edges, significantly mitigating local overheating.

The corresponding temperature-time profiles further quantify this behavior. The 70 wt% composite film demonstrates the fastest thermal response, reaching

thermal equilibrium much more rapidly than the neat polymer. More importantly, under the same heating power, the equilibrium surface temperature of the composite is lower than that of pure PVA, indicating a higher heat transfer rate to the surrounding environment. This superior heat dissipation performance is a direct consequence of the optimized microstructural design: the densely packed, horizontally aligned 4 µm BNNSs form continuous phonon highways with minimized interfacial resistance and exhibit a significant performance enhancement compared to previously reported studies (Table 1).

Table 1 Thermal conductivity values of our work and other published works about BNNS or BN-based polymer composites.

Filler composition and loading	Polymeric matrix	Tc (W/mk)	Relative Ref.
18.5 vol% BNNS	Epoxy	0.62	[32]
9.29 vol% BNNS	Epoxy	2.85	[33]
18.5 vol% BNNT	Epoxy	2.77	[34]
30 vol% h-BN@PDA	PVA	8.80	[35]
30 wt% BNNS	PVA	18.63	[36]
70 wt% BNNS	PVA	25.58	This work

In this work, we have achieved the spinnability of BNNSs at high loading levels, leading to a substantial enhancement in the in-plane thermal conductivity of the composite films compared to previous studies. These results conclusively demonstrate that the PVA/BNNS composite films are not only mechanically robust but also highly efficient in lateral heat spreading, making them ideal candidates for solving the thermal bottlenecks in lightweight, flexible, and high-power-density electronic devices.

CONCLUSION

In summary, we developed a lightweight, flexible, and electrically insulating PVA/BNNS composite film with an ultrahigh in-plane thermal conductivity of 25.58 $W\,m^{-1}\,K^{-1}$ at 70 wt% loading. By integrating co-electrospinning and hot-pressing, we elucidated the size effect of 2D fillers within 1D nanofibers. An optimized BNNS lateral size of 4 µm avoided the confinement mismatch and defects caused by larger fillers, ensuring perfect alignment to form a nacre-like brick-and-mortar structure. This architecture established continuous thermal pathways while preserving excellent mechanical flexibility, with practical cooling capabilities validated by infrared thermography. Ultimately, this synergistic optimization of filler dimension, orientation, and network density provides a robust theoretical framework for designing advanced flexible thermal management materials.

Acknowledgements: The authors gratefully acknowledge financial support from the Innovation Yongjiang 2035 Key R&D Plan International Cooperation Project (2024H027) and the Ningbo Youth Science and Technology Innovation Leading Talent Program (2023QL041).

REFERENCES

1. Li M, Li SX, Zhang ZH, Su CJ, Wong B, Hu YJ (2025) Advancing thermal management technology for power semiconductors through materials and interface engineering. *Acc Mater Res* **6**, 563–576.
2. Shrestha R, Li PF, Chatterjee B, Zheng T, Wu XF, Liu ZY, Luo TF, Choi S, et al (2018) Crystalline polymer nanofibers with ultra-high strength and thermal conductivity. *Nat Commun* **9**, 1664.
3. Xu XF, Chen J, Zhou J, Li BW (2018) Thermal conductivity of polymers and their nanocomposites. *Adv Mater* **30**, e1705544.
4. Hu FG, Li MH, Li PF, Zeng JS, Wang TG, Li JP, Wang B, Wu C, et al (2024) High-performance multifunctional nanopapers with superior mechanical strength, electromagnetic interference shielding, and thermal management for next-generation electronics. *Adv Funct Mater* **35**, 2418899.
5. Feng CP, Wei F, Sun KY, Wang Y, Lan HB, Shang HJ, Ding FZ, Bai L, et al (2022) Emerging Flexible thermally conductive films: Mechanism, fabrication, application. *Nanomicro Lett* **14**, 127.
6. Li ZY, Sun Y, Hu FY, Liu D, Zhang XP, Ren JN, Guo H, Shalash M, et al (2025) An overview of polymer-based thermally conductive functional materials. *Mater Sci Technol* **218**, 191–210.
7. Lu XH, Liu Ji, Shu C, Zhang SC, Zhao HY, Zhang Y, Wang QL, Yu ZZ, et al (2024) Densifying conduction networks of vertically aligned carbon fiber arrays with secondary graphene networks for highly thermally conductive polymer composites. *Adv Funct Mater* **35**, 2417324.
8. Zha JW, Wang F, Wan B (2025) Polymer composites with high thermal conductivity: Theory, simulation, structure and interfacial regulation. *Prog Mater Sci* **148**, 101362.
9. Jiong SY, Kim J, Kim K, Choi Y, Lee J, Lee J, Noh D, Park J, et al (2025) Electrostatically engineered thermal interface materials with multiscale boron nitride-alumina-nanodiamond fillers in polyvinyl alcohol composites for tailored anisotropic thermal conductivities. *Adv Compos and Hybrid Mater* **8**, 321.
10. Lin ZH, Sun ZJ, Fu WB, Lin YC, Moon K, Wong C (2025) Thermally conductive and electrically insulative alumina/epoxy composites for advanced electronic packaging applications: A comprehensive review of filler morphologies and surface modifications. *Mater Today* **86**, 393–413.
11. Yan QW, Dai W, Gao JY, Tan X, Lv L, Ying JF, Lu XX, Lu JB, et al (2021) Ultrahigh-aspect-ratio boron nitride nanosheets leading to superhigh in-plane thermal conductivity of foldable heat spreader. *ACS Nano* **15**, 6489–6498.
12. Alam FE, Dai W, Yang MH, Du SY, Li XM, Yu JH, Jiang N, Lin CT (2017) *In situ* formation of a cellular graphene framework in thermoplastic composites leading to superior thermal conductivity. *J Mater Chem A* **5**, 6164–6169.
13. Bai X, Meng YH, Zhou FY, Ge C, Sun DD, Yang DH, Jiang XF, Dai PC, et al (2024) Enhanced thermal conductivity of polymeric composites with BN@C hybrid fillers. *Mater Chem C* **12**, 15965–15974.

14. Kwon OH, Ha T, Kim DG, Kim BG, Kim YS, Shin TJ, Koh WG, Lin HS, et al (2018) Anisotropy-driven high thermal conductivity in stretchable poly(vinyl alcohol)/hexagonal boron nitride nanohybrid films. *ACS Appl Mater Interfaces* **10**, 34625–34633.
15. TabkhPaz M, Shajari S, Mahmoodi M, Park DY, Suresh H,Park SS (2016) Thermal conductivity of carbon nanotube and hexagonal boron nitride polymer composites. *Composites Part B Eng* **100**, 19–30.
16. Wang MJ, Jiao ZY, Chen YP, Hou X, Fu L, Wu YM, Li SY, Jiang N, et al (2018) Enhanced thermal conductivity of poly(vinylidene fluoride)/boron nitride nanosheet composites at low filler content. *Compos Part A Appl S* **109**, 321–329.
17. Li X, Wu B, Lv Y, Xia R, Qian JS (2025) Customized low heat resistance interfacial structure endowing multifunctional composite with excellent thermal conductivity. *Chem Eng J* **503**, 158246.
18. Wang YL, Xu LS, Yang Z, Xie H, Jiang PQ, Dai JQ, Luo W, Yao YG, et al (2017) High temperature thermal management with boron nitride nanosheets. *Nanoscale* **10**, 167–173.
19. Wang SG, Fan P, Liu WB, Hu B, Guo JX, Wang ZZ, Zhu SK, Zhao YP, et al (2024) Research progress of flexible electronic devices based on electrospun nanofibers. *ACS Nano* **18**, 31737–31772.
20. Yanar N, Kim TYS, Jung J, Dinh DK, Choi K, Pornea AG, Yadav D, Hanif Z, et al (2024) Boron nitride nanotube-aligned electrospun PVDF nanofiber-based composite films applicable to wearable piezoelectric sensors. *ACS Appl Nano Mater* **7**, 11715–11726.
21. Zeng QZ, Zhang L, Zhang JH, Zhang AM (2023) Thermo-conductive, air-permeable, and hydrophobic sulfonated poly(styrene-ethylene/butylene-styrene)/boron nitride nanosheet nanofiber membranes for wearables via one-step electrospinning. *ACS Appl Polym Mater* **5**, 4868–4878.
22. Huang X, Li ZD, Li YF, Wu XF, Liu CQ, Xie HQ, Yu W (2024) Thermally conductive boron nitride nanosheets on electrospun thermoplastic polyurethane for wearable janus-type fabrics with simultaneous thermal and moisture management. *ACS Appl Nano Mater* **7**, 8229–8237.
23. Fan L, Zhang S, Zhao GJ, Fu Q (2021) Constructing fibrillated skeleton with highly aligned boron nitride nanosheets confined in alumina fiber via electrospinning and sintering for thermally conductive composite. *Compos Part A Appl S* **143**, 106282.
24. Chen Y, Liu YJ, Liu XY, Li PL, Li Z, Jiang PK, Huang XY (2024) On-demand preparation of boron nitride nanosheets for functional nanocomposites. *Small Methods* **8**, e2301386.
25. Liu Z, Sun XY, Xie JL, Zhang X, Li JH (2022) Interfacial thermal transport properties and its effect on thermal conductivity of functionalized BNNS/epoxy composites. *Int J Heat Mass Transfer* **195**, 123031.
26. Chen Q, Wang X, Liang JY, Zhang TT, Jiang XW, Liu PF (2024) Synthesis of PVA@S-BNNSs flexible fiber backbone by electrostatic spinning assisting the construction of excellent ductile epoxy thermal interface materials. *Compos Sci Techno* **247**, 110435.
27. Yang X, Qin L, Wang LC, Ding RM, Shi LY, Lv BL (2018) Scalable synthesis of quasi-monodispersed BN colloidal nanocrystals by "solvent cutting" and their anti-electrochemical corrosion coating. *Chem Eng J* **333**, 191–199.
28. Zhan K, Chen Y, Xiong Z, Zhang Y, Ding S, Zhen F, Liu Z, Wei Q, et al (2024) Low thermal contact resistance boron nitride nanosheets composites enabled by interfacial arc-like phonon bridge. *Nat Commun* **15**, 2905.
29. Guo GL, Liu YJ, Ding YF, Liu WJ, Zhu GM, Hao XL, Huang XY, Xia JF, et al (2024) Flexible yet impermeable composites with wrinkle structured BNNSs assembling for high-performance thermal management. *npj Flexible Electron* **8**, 34.
30. Jing L, Cheng R, Tasoglu M, Wang ZX, Wang QX, Zhai H, Shen S, Cohen-karni T, et al (2023) High thermal conductivity of sandwich-structured flexible thermal interface materials. *Small* **19**, e2207015.
31. Wang TZ, Chi H, Zhao DY, Dong JG, Li M, Jiang ZH, Zhang YH (2025) A highly thermally conductive yet electrically insulating boron nitride nanosheets/polyetherimide composite with oriented structure. *Compos Part A Appl S* **188**, 108581.
32. Huang XY, Zhi CY, Jiang PK, Golberg D, Bando Y, Tanaka T (2012) Polyhedral oligosilsesquioxane-modified boron nitride nanotube based epoxy nanocomposites: An ideal dielectric material with high thermal conductivity. *Adv Funct Mater* **23**, 1824–1831.
33. Han JK, Du GL, Gao WW, Bai H (2019) An anisotropically high thermal conductive boron nitride/epoxy composite based on nacre-mimetic 3D network. *Adv Funct Mater* **29**, 1900412.
34. Shen H, Guo J, Wang H, Zhao N, Xu J (2015) Bioinspired modification of h-BN for high thermal conductive composite films with aligned structure. *ACS Appl Mater Interfaces* **7**, 5701–5708.
35. Sun JY, Zhao YN, Yang ZG, Shen JL, Cabrera E, Lertola, Yang W, Zhang D, et al (2018) Highly stretchable and ultrathin nanopaper composites for epidermal strain sensors. *Nano Tech* **29**, 355304.
36. Yang XT, Guo YQ, Han YX, Li Y, Ma TB, Chen MJ, Kong J, Zhu JH, et al (2019) Significant improvement of thermal conductivities for BNNS/PVA composite films via electrospinning followed by hot-pressing technology. *Compos Part B Eng* **175**, 1359–8368.